Journal of Applied Polymer Science

Thermal and dielectric properties of polycarbonatediol polyurethane

Pilar Ortiz-Serna,[1] Marta Carsí,[1] Belén Redondo-Foj,[1] María Jesús Sanchis,[1] Mario Culebras,[2] Clara María Gómez,[2] Andrés Cantarero[2]

[1]Departamento de Termodinámica Aplicada, E.T.S.I.I., Instituto de Tecnología Eléctrica Universitat Politècnica de Valencia, 46022 Valencia, Spain

[2]Condensed Matter and Polymers Group, Materials Science Institute, University of Valencia, 46071 Valencia, Spain

Correspondence to: M. J. Sanchis (E-mail: jsanchis@ter.upv.es)

ABSTRACT: The dielectric relaxation behavior of segmented polyurethane has been studied using Broad-Band Dielectric Spectroscopy in the frequency domain, 10^{-2} to 10^{8} Hz, and in the temperature range of −120 to 140°C. The spectra show three secondary processes (δ, γ, and β) followed by the α relaxation and conductive processes. The Havriliak-Negami (HN) phenomenological equation was used in order to characterize all the processes. The δ, γ, and β relaxations are probably associated with (i) local motions of the main chain (ii) motions of the carbonate group in the soft phase and (iii) reorientational motions of water molecules. The microphase separated morphology associated with soft and hard domains is reflected in the dielectric spectra, at high temperatures, by the presence of the Maxwell-Wagner-Sillars (MWS) interfacial polarization process. © 2015 Wiley Periodicals, Inc. J. Appl. Polym. Sci. **2015**, *132*, 42007.

KEYWORDS: dielectric properties; polyurethanes; structure-property relations

Received 18 September 2014; accepted 17 January 2015

DOI: 10.1002/app.42007

INTRODUCTION

Polyurethanes are one of the most versatile materials since they can behave as elastomers, thermoplastics, or thermoset polymers depending on the different reactants and synthesis conditions selected. They are extensively used as foams, elastomers, coatings, sealants, and adhesives in different applications.[1–5] Segmented polyurethane elastomers (TPU) are linear block copolymers formed by thermodynamically incompatible segments named as soft and hard domains. The soft segment is a polyol of molecular mass between 500 and 3000 g mol^{-1} that provides high flexibility at room temperature. The hard segment is formed by a diisocyanate and a low-molecular-weight diol which providing physical crosslink sites through strong intermolecular hydrogen bonding.[6,7] The morphological, physical, chemical, and mechanical properties of TPUs range in a wide spectrum depends on the hard segment formulation and content, molecular structure of soft segment, and manufacturing conditions. In contrast, polycarbonatediol (PCD) derived TPUs depict improved water and organic solvent resistance, high mechanical strength, and high heat-resistance, at the expense of an increase in the price.[8–10] In the last years, we have been working in the identification and functional characterization of improved efficiency of PCD based TPUs[7,11–13] since few studies have been published.

Dielectric spectroscopy (DS)[14–16] represents a powerful tool for investigating the polymer dynamics. This technique allows studying the dielectric properties in a broad temperature and frequency range. The dielectric behavior can be directly related to phase-separated morphologies and is a suitable tool to understand the mechanisms underlying the physical properties. Novel materials with different phase-separated morphology have been prepared and the influence of morphologies on the molecular dynamics has been analyzed.[17–24]

The objective of the present study is to analyze the effect of the hard/soft domains in the molecular dynamics of polycarbonatediol polyurethane. In order to analyze the molecular dynamics of this material, we have employed the dielectric spectroscopy because it is a useful technique that allows the study of dynamics over a very broad range of frequencies, both in the glassy and rubbery states.

EXPERIMENTAL

Materials

Polyurethane solutions were obtained by a standard polymerization method based on the two-step process in dimethylacetamide;[7,13,25] 4,4′-diphenylmethane diisocyanate (MDI), 1,4-butanediol (BD), and dimethyl acetamide (DMAc), as solvent, were purchased from Aldrich (Barcelona, Spain). The macrodiol

Polyhexamethylene–pentamethylene carbonatediol (PH100) of molar mass 1000 g mol^{-1} and glass transition temperature of −51.32°C, was kindly supplied by UBE Chem Eur. (Castellón, Spain). All materials were kept in a dry box to avoid humidity. The molar ratio used for this study was PH100 : BD : MDI = 1 : 2 : 3 in mole ratio. Details on synthesis and sample preparation are given in previous articles.[7,13]

Modulated Differential Scanning Calorimetry Measurements

MDSC of polyurethane was carried out using a TA Instruments DSC Q-20 with a refrigerated cooling stage calibrated with indium and sapphire. The measurement was done in nonhermetic aluminium pans using an empty one as the reference cell from −80°C to 220°C at a heating rate of 3°C min^{-1}. The sample mass was 7.0 ± 0.1 mg. The test was performed under a 50 mL min^{-1} flow of nitrogen to prevent oxidation. The modulation temperature amplitude was ±1°C with a period of 60 s. The glass transition temperature (T_g) was evaluated as the intersection of the base line of the glassy region with the tangent to the endotherm in the middle point.

Dielectric Measurements

The experimental dielectric behavior of PUPH was studied with a Novocontrol Broadband Dielectric Spectrometer (Hundsagen, Germany) consisting of an AC-Impedance analyzer (Alpha-A analyzer) in combination with the ZGS Alpha Active sample cell test interface to carry out measurements from 5×10^{-2} to 3×10^6 Hz and an radiofrequency (RF) impedance analyzer (Agilent 4991A) in combination with a RF-extension line, BDS 2300 mounting rack and RF sample cell BDS 2200 to carry out the measurement in the frequency range of 10^6 to 10^8 Hz. In the latter case the complex permittivity was obtained by measuring the reflection coefficient at a particular reference plane. Before performing the measurements, the calibrations recommended by Novocontrol Technologies were carried out with the support of the Novocontrol WinDETA software. In order to allow the replication of the results at high frequencies, we performed the calibration of the entire system before the experimental measurements, i.e. the line and the RF sample cell. Thus, the line was calibrated using the calibration kit supplied with the RF impedance analyzer (short, open, 50hm, and low loss capacitor test units). For the cell calibration, we performed a short and open electrode arrangement within the RF sample cell. The measurements were carried out in inert N_2 atmosphere between −120°C and 140°C. The temperature was controlled by a nitrogen jet (QUATRO from Novocontrol), with a temperature uncertainty of 0.1°C during every single sweep in frequency. Moulded disc shaped sample of about 0.1 μm thicknesses and 20 mm diameter was used. The experimental uncertainty was better than 5% in all cases.

RESULTS AND DISCUSSION

Modulated Differential Scanning Calorimetric Measurements

MDSC was used in order to characterize the thermal behavior of the polyurethane. This technique applies a sinusoidal temperature oscillation and separates the heat flow in two components, reversing and nonreversing heat flow. The reversing signal provides a high resolution to determine the glass transition temperature and the nonreversing signal is very useful to characterize the time-dependent behavior, such as enthalpy relaxation and recrystallization. Figure 1 shows MDSC curves for PUPH. Two transitions are observed in the reversing signal. The first one is a glass transition temperature at 1.2°C, with heat capacity $\Delta C_p = 0.149$ J $g^{-1}°C^{-1}$, which is related to the amorphous part of the polyurethane. The T_g increases 59.4° with respect to that of the macrodiol (PH100, −51.32°C), indicating a great degree of miscibility of the soft segment with the hard segment, as commonly reported.[1,7,8,13,25–27] Miscibility between hard and soft segments results from their ability to establish hydrogen-bonding interactions.[28] The second transition is an endotherm peak at 160°C, which is related to the melting of hard domains.[8,29–32]

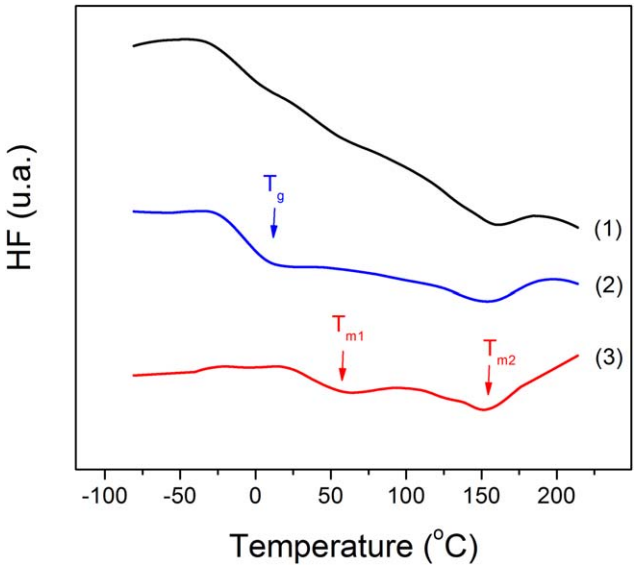

Figure 1. Modulated differential scanning calorimetry curves of PUPH. (1) Total heat flow; (2) reversing component; and (3) nonreversing component. [Color figure can be viewed in the online issue, which is available at wileyonlinelibrary.com.]

On the other hand, two transitions are observed in the nonreversing signal. The first one, located around 58°C, corresponds to the melting of a domain formed during aging as explained by other authors, since it not appears in the reversing signal.[31,32] This endothermic peak in the nonreversing curve is related to enthalpic relaxation of hard segments with short-range ordered structures. The second transition is the same endotherm peak observed in the reversing signal at 160°C, corresponding to the melting of hard domains. These endotherms could be attributed to the occurrence of nonreversible recrystallization related with the thermal history of the sample. An increase in the bonded urethane contribution with a progressively increase in the melting temperatures and enthalpies due to the formation of larger crystalline structures of hard segment have been reported and observed by atomic force microscopy and X-ray diffraction. Phase segregation structure of hard/soft-segment microdomains surface is dependent on the macrodiol molar mass and hard segment content, as reported[7,8,12,13,20,26,27]

The thermal conductivity was determined by MDSC, according to the ASTM E1952-11 standard method. This is ideal for measuring thermal conductivity of polymeric materials with values

between 0.1 and 1.0 W m^{-1} K^{-1}. A value of 0.23 ± 0.02 W m^{-1} K^{-1} was obtained for the thermal conductivity of PUPH in good agreement with previous results.[33] The thermal diffusivity was calculated using the following equation (ASTM E1952-11):

$$\alpha = \frac{\pi \cdot k \cdot d^2 \cdot L}{4 \cdot C_p \cdot m} \quad (1)$$

where κ is the thermal conductivity; d the specimen diameter; L sample length; C_p the heat capacity; and m the sample mass. A value of 0.17 ± 0.02 mm^2 s^{-1} was obtained for the thermal diffusivity of PUPH.

Dielectric Measurements

Figure 2 shows three-dimensional (3D) representations of the real and imaginary components of the complex dielectric permittivity for the PUPH film, in the range of 10^{-2} to 10^8 Hz and temperature window of −120 to 140°C.

All the isochrones showing the variation of the dielectric permittivity ε', display the same pattern in the sense that they present two steps, a low temperature step associated with the glass rubber transition or α relaxation followed by a second step at higher temperature, associated with the Maxwell-Wagner-Sillars (MWS) relaxation.[34–36] Finally, an important increase of the permittivity, related to the electrode polarization (EP) effects, it is observed. EP originates from the accumulation of charges at the electrode-polymer interface whereas the interfacial polarization or MWS process is due to the build-up of charges at the interfaces of the components of the heterogeneous systems.[37] As discussed above, the PUPH is a heterogeneous system due to the existence of microphase separation associated with the soft and hard microdomains. The polarization of microdomains resulting from the separation of the hard and soft segments of PUPH chains can cause the accumulation of charges, a process that can be attributed to the different conductivity paths between the soft and hard microdomains. The evidence of the presence of these microdomains in the PUPH under study has been demonstrated by means of the WAXS measurement results.[12]

The isochrones corresponding to the dielectric loss ε'' clearly present two relaxational zones. In the low-temperature region, we can observe the presence of three secondary relaxations, labeled as δ, γ, and β processes, presumably associated with side chain motions (see inset in Figure 2). In the high-temperature zone the spectrum present an ostensible α relaxation associated with the glass transition temperature followed by a rather sharp increase as temperature increases as a result of the strong contribution of the conductivity. The contribution of the polarization, produced at the electrode-polymer interface, to the dielectric loss scales with frequency dependence as ω^{-s}, where usually s is a parameter close to unity.

PUPH is a typical system in which charge contributions to the dielectric permittivity are important at low frequencies. Therefore, it is also convenient to analyze the results in terms of the complex dielectric modulus $M^* = 1/\varepsilon^*$, a variable very sensitive to charge transport.[38] This formalism has several advantages:[39] (i) it allows the determination of the dc conductivity from the M'' spectra, (ii) conductive effects usually do not mask the features of the spectra, and (iii) the results of the dielectric analysis are seemingly analogous to the mechanical modulus of solids. So, Figure 3 plots the mechanical (E'')[12] and dielectric loss modulus (M'') as a function of temperature at 1 Hz. Both spectra clearly present two relaxational zones. In the low-temperature region, we can observe the presence of several secondary relaxations, presumably associated with local motions. In the high-temperature region, both spectra show an ostensible α relaxation. Moreover, only in the dielectric spectrum two processes associated with the conductivity phenomena (MWS and EP) are observed.

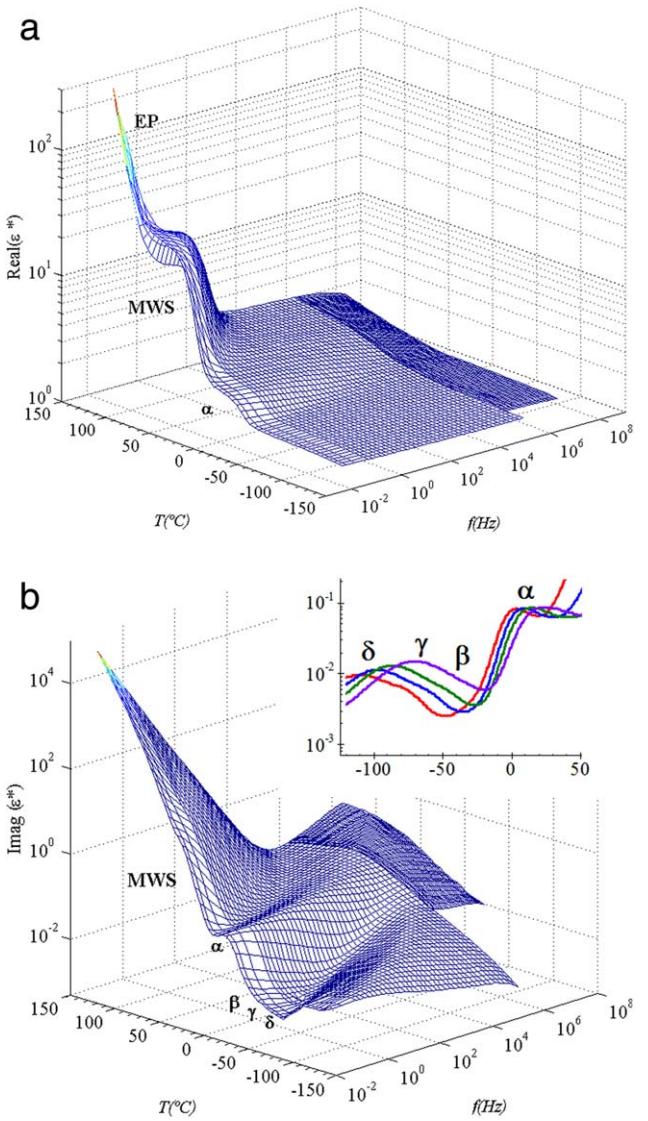

Figure 2. Three-dimensional representation of the dielectric permittivity of PUPH in the temperature range of −120 to 140°C, step 5°C. Inset: zoom of the low temperature region. [Color figure can be viewed in the online issue, which is available at wileyonlinelibrary.com.]

The analysis of the dielectric spectrum was made by using the phenomenological equation of Havriliak-Negami (HN).[40,41] This equation relates the complex permittivity (ε^*) to the frequency by

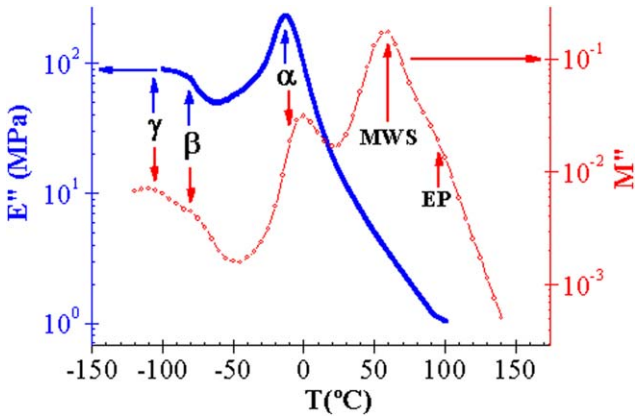

Figure 3. Temperature dependence of the dielectric loss modulus and loss mechanical modulus at 1 Hz for PUPH film. [Color figure can be viewed in the online issue, which is available at wileyonlinelibrary.com.]

$$\varepsilon^*_{\mathrm{dip}(\omega)} = \varepsilon_\infty + \frac{\varepsilon_0 - \varepsilon_\infty}{\left[1+(j\omega\tau_{\mathrm{HN}})^{a_{\mathrm{HN}}}\right]^{b_{\mathrm{HN}}}} \quad (2)$$

where the subscripts ε_0 and ε_∞ are, respectively, the relaxed ($\omega \to 0$) and unrelaxed ($\omega \to \infty$) dielectric permittivities, and τ_{HN} is the characteristic relaxation time associated with the relaxation. The shape parameters a_{HN} and b_{HN} fulfil the condition $0 < a_{\mathrm{HN}} b_{\mathrm{HN}} \leq 1$, and for a Debye process $a_{\mathrm{HN}} = b_{\mathrm{HN}} = 1$. These parameters are related, respectively, to the departure of the complex ε'' versus ε' plot from a semi-circumference, at low frequencies, and to the skewness of the plot along a straight line, at high frequencies.[42]

The analysis of the dielectric spectrum was carried out in the two zones: (i) high frequency zone where three secondary processes are intimately overlapped and (ii) low frequency zone where the α process is overlapped with a secondary process, at high frequency values, and with MWS and EP processes at low frequency values.

In the high frequency zone, an additive rule for the permittivity was assumed,[43] i.e., the analysis of the dielectric spectra was carried out by means of the addition of two HN functions corresponding to β and γ processes (from −45 to −70°C) and to δ and γ processes (from −80 to −110°C). Both HN functions were used with $b_{\mathrm{HN}} = 1$. When $b_{\mathrm{HN}} = 1$, eq. (2) reduces to the Cole-Cole equation,[44] which describes processes with symmetric distribution of relaxation times, characteristic of the secondary relaxations.

The HN parameters of the three secondary relaxations were determined at several temperatures from a multiple nonlinear regression analysis of the dielectric loss. The three characterizing peak parameters ($\Delta\varepsilon_i$, $\tau_{\mathrm{HN}i}$, $a_{\mathrm{HN}i}$) were allowed to vary. As an example, Figure 4 plots the experimental data, the global fit and the deconvolution obtained in the fitting procedure of the loss factor at −45 and −105°C.

In the low frequency zone, where the conductive process is dominant, we have included a new term in order to characterize the spectrum: $\varepsilon^*(\omega) = \varepsilon^*_{\mathrm{dip}} + \varepsilon^*_{\mathrm{cond}}$ with $\varepsilon^*_{\mathrm{cond}}(\omega) = j(\sigma/\varepsilon_0\omega^s)$, where $\varepsilon_0 = 8.854$ pF m^{-1} is the dielectric permittivity of vacuum, σ is the conductivity arising from charges transport at the liquid-electrode interface, and s is a constant ($s \leq 1$). The dielectric analysis in this region was carried out by means of three HN functions and a conductive function, corresponding in decreasing order of frequency to γ, α, MWS, and EP processes. So, the fit parameters were determined at several temperatures from a multiple nonlinear regression analysis of the experimental data by using the following expression

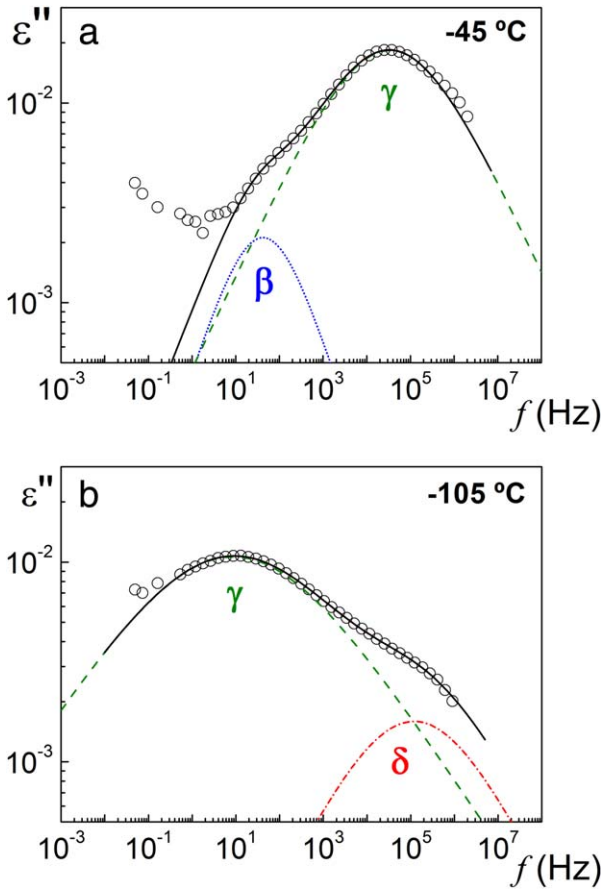

Figure 4. Experimental dielectric loss factor data (circle), global fit (continuous line), and individual relaxations (dashed lines) as a function of frequency at −45 and −105°C. [Color figure can be viewed in the online issue, which is available at wileyonlinelibrary.com.]

$$\varepsilon'' = \mathrm{Im}\left[\varepsilon_\infty + \sum_{i=1}^{3} \frac{\Delta\varepsilon_i}{\left(1+(i\omega\tau_i)^{a_{\mathrm{HN}i}}\right)^{b_{\mathrm{HN}i}}} + j\left(\frac{\sigma}{\varepsilon_0\omega^s}\right)\right] \quad (3)$$

Figure 5 shows, as an example, the deconvolution of the experimental data at 30°C.

The HN and ionic conductivity fit parameters obtained for all the processes observed in PUPH sample are plotted in Figures 6 to 8.

Figure 6 shows the a_{HN} shape parameter of the PUPH relaxation processes. For the secondary relaxations, it is observed a slightly increase of the a_{HN} values with the temperature. For the α relaxation, a low temperature dependence of the a_{HN} parameter value was observed, whereas the b_{HN} parameter increases with the temperature obtaining a value of 1 for the highest temperatures. In the case of the MWS process, the a_{HN} and b_{HN}

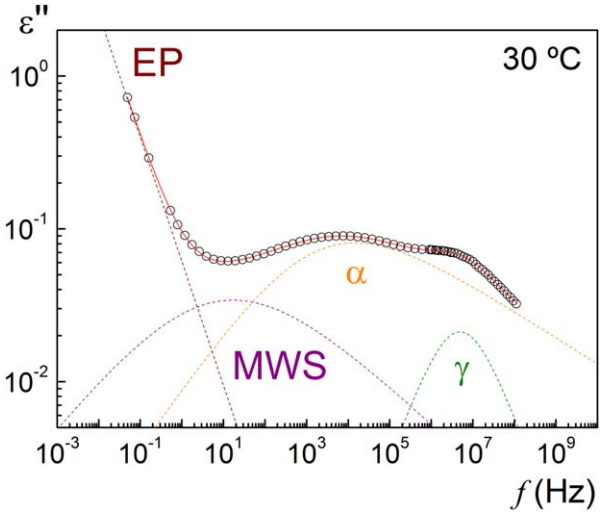

Figure 5. Experimental dielectric loss factor data (circle), global fit (continuous line), and individual relaxations (dashed lines) as a function of frequency at 30°C. [Color figure can be viewed in the online issue, which is available at wileyonlinelibrary.com.]

parameters show also low temperature dependence. At high temperatures and low frequencies the spectrum is very complicated, appearing closely overlapping dielectric relaxation processes (α and γ) and conductive processes (MWS and EP). For this reason, it is possible that the sharp variations with temperature obtained for some of them could be related to the complexity of the fitting procedure with a large number of variable parameters.

As we can observe, the secondary relaxation detected in the high temperature zone is well correlated with the γ process previously characterized in the low temperature and high frequency range.

Figure 7 shows the temperature dependence of the relaxation strength for the PUPH relaxation processes. Regarding the secondary relaxations, Δε of the γ process slightly increases with temperature, following the classical trends. On the other hand, the strength values of the δ and β processes are lower than that corresponding to the γ process and remains practically constant with temperature.

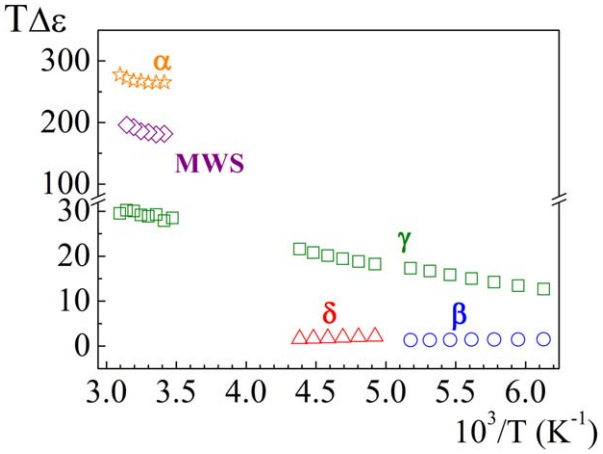

Figure 7. Temperature dependence of the strengths of the δ (triangles), γ (square), β (circles), α (star), and MWS (diamond) relaxations for PUPH. [Color figure can be viewed in the online issue, which is available at wileyonlinelibrary.com.]

The α-relaxation strength remains practically constant with temperature, following the classical trend. The thermal energy disturbs the alignment of the molecule dipoles that intervene in the cooperative motions and give rise to the relaxation. On the other hand, the strength of the MWS process also remains practically constant with temperature.

Figure 8 shows the temperature dependence of the relaxation times associated with the peak maxima of the PUPH relaxation processes.

The characteristic relaxation time τ_{HN} is related to the relaxation times associated with the loss of peak maxima, τ_{max}, by[45]

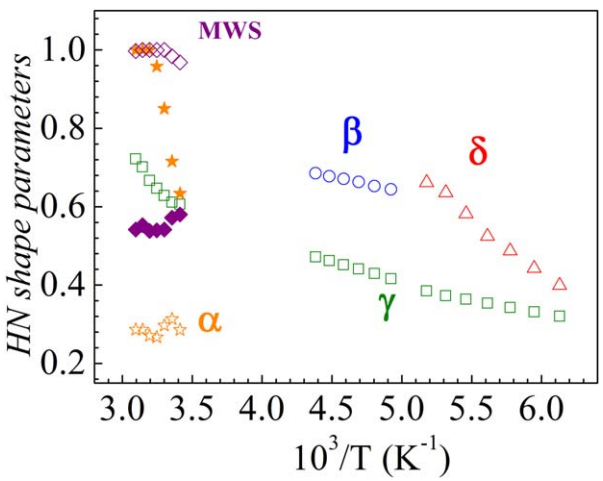

Figure 6. Temperature dependence of the shape parameters, a_{HN} (open) and b_{HN} (solid) from eq (2), of the δ (triangles), γ (square), β (circles), and α (star) relaxations for PUPH. [Color figure can be viewed in the online issue, which is available at wileyonlinelibrary.com.]

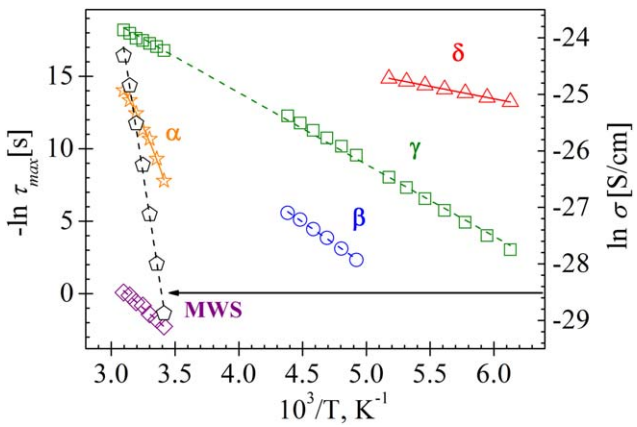

Figure 8. Arrhenius plot for the δ (triangles), γ (square), β (circles), α (star), MWS (diamond), and ionic conductivity (pentagon) processes for PUPH. [Color figure can be viewed in the online issue, which is available at wileyonlinelibrary.com.]

Table I. Characteristic Parameters of the Dipolar and Conductivity Processes for PUPH

	σ_{dc}	MWS	α	β	γ	δ
$\log_{10}\tau_0$ (s)		-10.6 ± 0.1	-11.9 ± 0.2	-14.0 ± 0.3	-14.6 ± 0.1	-10.3 ± 0.1
D_0		-	5.6 ± 0.1	-	-	-
T_v (K)		-	228.0 ± 0.2	-	-	-
E_a (kJ mol^{-1})	121.6 ± 3.1	64.9 ± 6.0	-	50.3 ± 1.1	41.2 ± 0.4	14.2 ± 0.1
ϕ_g/B		-	0.039 ± 0.001	-	-	-
$\alpha \times 10^4$ (K^{-1})		-	7.87 ± 0.21	-	-	-
$\log_{10}\sigma_0$ (S cm^{-1})	-11.18 ± 0.5					

$$\tau_{max} = \tau_{HN}\left[\frac{\sin(\pi a_{HN} b_{HN}(2+2b_{HN}))}{\sin(\pi a_{HN}(2+2b_{HN}))}\right]^{1/a_{HN}} \quad (4)$$

It can be seen that the three secondary relaxations exhibit an Arrhenius (ARRH) behavior: $\tau_{max} = \tau_0 \cdot \exp[E_a/RT]$. The fit parameters to the ARRH equation are compiled in Table I. The activation energy values obtained for the γ and δ processes (41.2 ± 0.4 and 14.2 ± 0.1 kJ mol^{-1}, respectively) are of the same order of magnitude than those obtained for other related polyurethanes.[46] These processes are probably associated with the local motions of the main chain and/or the carbonate group in the soft phase. On the other hand, a similar weaker and slower β process has been observed in a wide variety of water-contained systems. It has been associated with reorientational motions of the water molecules.[47–49] This process has also been observed in other polyurethane systems,[46] although the samples had been extensively dried prior to the dielectric measurements, like in the case of our samples.

The temperature dependence of the relaxation time for the α-process follows a Vogel-Tammann-Fulcher-Hesse (VTFH) behavior.[50–56]

$$\tau = \tau_0 \cdot \exp\left(\frac{D_0 \cdot T_v}{T - T_v}\right) \quad (5)$$

where τ_0 is a pre-exponential factor identified sometimes with vibrational lifetimes[57] (whose value is of the order of 10^{-14} s), D_0 is the strength coefficient,[58,59] and T_v is the Vogel temperature, currently associated with the temperature at which the entropies of the glassy system and the crystal are similar, i.e. when the configurational entropy of the glassy system is 0. The fit parameters of eq. (5) to the Arrhenius plot (see Figure 8) are summarized in Table I. As usual, the results for T_v are nearly 50 K below those of T_g. Moreover, the fragility parameter obtained for this polymer is lower than 10, the frontier that separates fragile ($D_0 < 10$) from strong ($D_0 > 10$) glasses.[58–62]

By comparing eq. (5) with the Doolittle expression,[63,64] the fraction of free volume at the glass transition temperature, ϕ_g/B, and the free volume expansion coefficient $\alpha_f = (1/V)(\partial V/\partial T)_p$ are estimated from the following expressions

$$\frac{\phi_g}{B} = \frac{T_g - T_v}{D_0 \cdot T_v}$$
$$\frac{\alpha_f}{B} = \frac{1}{D_0 \cdot T_v} \quad (6)$$

According to the Cohen-Turbull theory, B is a parameter close to unity related to the ratio between the critical volume for a relaxation process to take place and the volume of the segments involved in the process.[65,66] Assuming $B = 1$, the value of the relative free volume ϕ_g at T_g is 0.039 ± 0.001, whereas the value of the thermal expansion coefficient of the free volume α_f at T_g is $7.87 \pm 0.21 \times 10^{-4}$ K^{-1}. It is worth noting that the value of ϕ_g is slightly higher than the value reported for this quantity for most flexible polymers. Presumably, this is due to the fact that the relaxation curves only extend over a rather limited span of frequency and temperature windows. On the other hand, the thermal expansion coefficient of the free volume α_f at T_g is similar to the value reported for the most flexible polymers,[67] which lies in the vicinity of 5×10^{-4} K^{-1}.

The temperature dependence of the relaxation time for MWS process was ARRH-type. The characterized parameters obtained from the fitting of MWS relaxation are summarized in Table I.

In our analysis, the s parameter of eq (3) was equal to one for all analyzed isotherms. Moreover, the conductivity values (σ) obtained at several temperatures show an Arrhenius behavior $\sigma_{dc} = (0(\exp[-(Ea(RT]$ (see Figure 8), from which we have evaluated the activation energy obtaining a value of 121.6 ± 3.1 kJ mol^{-1}.

In order to analyze the conductive processes, it is interesting to investigate the dependence on frequency and temperature of the ac conductivity σ'_{ac} ($=2\pi f e_0 \varepsilon''$). Figure 9 shows the frequency plots of σ'_{ac} at temperatures between 30 and 140°C (step 10°C) and the frequency dependence of σ'' at 140°C.

As we can see, σ'_{ac} changes drastically with temperature and frequency. At temperatures higher than 70°C, a plateau (a region where σ'_{ac} is frequency independent) can be clearly visualized in the plots. This behavior is the same as the respective one of "pure" dc conductivity. At higher frequencies, σ'_{ac} increase rapidly with increasing frequency. The transition region from dc (frequency independent) to ac (frequency dependent) conductivity shifts to higher frequencies with increasing temperature. As the temperature increases, the plateau is shifted to higher σ'_{ac} values, as expected for thermal activated conductivity.

Moreover, at high temperatures and low frequencies, σ'' decreases with decreasing frequency passing through a minimum and increasing again at the lowest frequencies. This behavior can be ascribed to electrode polarization (EP). As the frequency decreases, more and more charge carriers accumulate

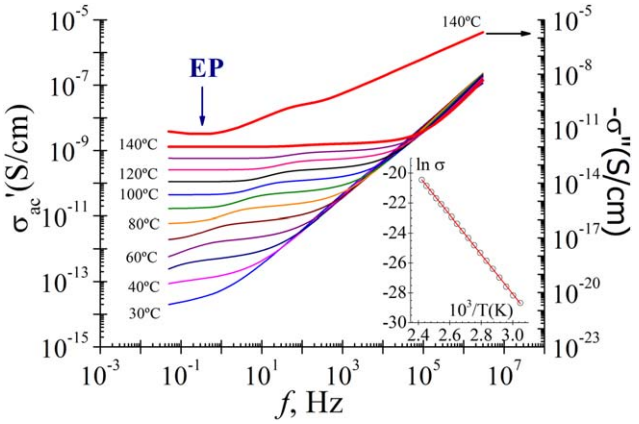

Figure 9. Values of ac conductivity against frequency for PUPH at temperatures in the range of 30°C to 140°C. Inset: Arrhenius plot associated with the dc conductivity. [Color figure can be viewed in the online issue, which is available at wileyonlinelibrary.com.]

at the interface between the sample and the electrodes, which leads to the drop in ac conductivity at low frequencies. The EP effect becomes increasingly important at high temperatures, reflecting the enhancement of the mobility of charge carriers.

As we can see in the inset of Figure 9, the temperature dependence of the dc conductivity values at several temperatures is described by the ARRH equation. These dc conductivity values are obtained from extrapolation to low frequencies of the frequency dependence of σ'. The corresponding Arrhenius plot is shown in the inset of Figure 9, and their corresponding activation energy and $\log_{10}\ \sigma_o$ S cm^{-1} are 118.5 ± 1.0 kJ mol^{-1} and 11.1 ± 0.2, respectively. These values are in accordance with those obtained by fitting of the experimental data to eq (3) (121.6 ± 3.1 kJ mol^{-1} and 11.2 ± 0.5, respectively).

CONCLUSIONS

MDSC results indicate a great degree of miscibility between the soft and hard segment phases due to the observed increase in the T_g value of the PUPH with respect to the pure soft segment one, PH100. This increase in the soft segment temperature is related with increasing interactions between soft and hard segment thus increasing the miscibility between both phases. The glass transition temperature value obtained from MDSC and DRS are in good agreement. So, the obtained T_g value from MDSC was 1.2°C, whereas the obtained value from DRS (at 1 Hz) was 1.6°C. The endotherm transition at 160°C indicates a long-range ordering of the hard domains.

The relaxational behavior of the PUPH has been analyzed by using DRS. The spectrum exhibits five relaxations, in the range of frequencies and temperatures studied, named in decreasing order of frequency δ, γ, β, α, and MWS. The δ and γ processes are associated with local motions of the main chain and/or the carbonate group in the soft phase. The β process has been associated with reorientational motions of the water molecules and the α relaxation is related to the glass transition temperature. At lower frequencies it is observed a MWS process, related to the build-up of charges at the interfaces of soft and hard microdomains components of the PUPH heterogeneous system. The absence of this MWS process in the mechanical relaxational spectrum is indicative of the conductive origin of the process. Evidence of the presence of these microdomains in PUPH under study has been demonstrated by means of the WAXS measurement results.[12] Finally, at the lowest frequencies the loss permittivity spectrum is dominated by EP, a conductivity process related to the accumulation of charges at the electrodes-polymer interface. The contribution to the dielectric loss in the EP process scales as ω^s.

ACKNOWLEDGMENTS

This work was financially supported by the DGCYT through Grant MAT2012-33483. The authors thank UBE Chem. Corporation for supplying the polycarbonatodiol to synthesize the polyurethanes of this work.

REFERENCES

1. Lee, S. Thermoplastic Polyurethane Markets in the EU-Production, Technology, Applications and Trends a Report from Rapra's Industry Analysis and Publishing Group; iSmithers Rapra Publishing: Uitgewer, **1998**.
2. Szycher, M. Handbook of Polyurethanes; CRC Press: Washington DC, **1999**.
3. Oertel, G. Polyurethane Handbook, 2nd ed.; Hanser: New York, **1993**.
4. Prisacariu, C. Polyurethane Elastomers. From Morphology to Mechanical Aspects; Springer: New York, **2011**.
5. Król, P. *Prog. Mater. Sci.* **2007**, *52*, 915.
6. Strawhecker, K. E.; Hsieh, A. J.; Chantawansri, T. L.; Kalcioglu, Z. I.; Van Vliet, K. J. *Polymer* **2013**, *54*, 901.
7. Costa, V.; Nohales, A.; Félix, P.; Guillem, C.; Gómez, C. M. *J. Elast. Plast.* **2012**, *45*, 217.
8. Eceiza, A.; Martin, M. D.; de la Caba, K.; Kortaberria, G.; Gabilondo, N.; Corcuera, M. A.; Mondragon, I. *Polym. Eng. Sci.* **2008**, *48*, 297.
9. Kojio, K.; Nonaka, Y.; Masubuchi, T.; Furukawa, M. *J. Polym. Sci. Part B: Polym. Phys.* **2004**, *42*, 4448.
10. Tanaka, H.; Kunimura, M. *Polym. Eng. Sci.* **2002**, *42*, 1333.
11. Costa, V.; Muñoz, B.; Nohales, A.; Félix, P.; Gómez, C. M.; Guillem, C.; Latorre, J. *Revista de Plásticos Modernos* **2008**, *95*, 384.
12. Gómez, C. M.; Culebras, M.; Cantarero, A.; Redondo-Foj, B.; Ortiz-Serna, P.; Carsí, M.; Sanchis, M. J. *Appl. Surf. Sci.* **2013**, *275*, 295.
13. Costa, V.; Nohales, A.; Félix, P.; Guillem, C.; Gutiérrez, D.; Gómez, C. M. *J. Appl. Polym. Sci.* **2015**. DOI: 10.1002/APP.41704.
14. Kremer, F.; Schönhals, A. Broadband Dielectric Spectroscopy; Springer: Berlin, **2003**.
15. McCrum, N. G.; Read, B. E.; Williams, W. Anelastic and Dielectric Effects in Polymeric Solids; Dover Publications, Inc.: New York, **1991**; p 118.

16. Riande, E.; Díaz Calleja, R. Electrical Properties of Polymers; Marcel Dekker Inc.: New York, **2004**.
17. Pissis, P.; Georgoussis, G.; Bershtein, V. A.; Neagu, E.; Fainleib, A. M. *J. Non-Cryst. Solids* **2002**, *305*, 150.
18. Czech, P.; Okrasa, L.; Mechin, F.; Boiteux, G.; Ulanski, J. *Polymer* **2006**, *47*, 7207.
19. Okrasa, L.; Czech, P.; Boiteux, G.; Mechin, F.; Ulanski, J. *Polymer* **2008**, *49*, 2662.
20. Polizos, G.; Kyritsis, A.; Pissis, P.; Shilov, V. V.; Shevchenko, V. V. *Solid State Ionics* **2000**, *136*, 1139.
21. Castagna, A. M.; Fragiadakis, D.; Lee, H.; Choi, T.; Runt, J. *Macromolecules* **2011**, *44*, 7831.
22. Castagna, A. M.; Pangon, A.; Choi, T.; Dillon, G. P.; Runt, J. *Macromolecules* **2012**, *45*, 8438.
23. Fragiadakis, D.; Runt, J. *Macromolecules* **2013**, *46*, 4184.
24. Tsonos, C.; Apekis, L.; Zois, C.; Tsonos, G. *Acta Mater.* **2004**, *52*, 1319.
25. D'Arlas, B. F.; Rueda, L.; De la Caba, K.; Mondragon, I.; Eceiza, A. *Polym. Eng. Sci.* **2008**, *48*, 519.
26. Wang, C. B.; Cooper, S. L. *Macromolecules* **1983**, *16*, 775.
27. Fernández d 'Arlas, B.; Rueda, L.; De la Caba, K.; Mondragon, I.; Eceiza, A. *Polym. Eng. Sci.* **2008**, *48*, 519.
28. Lazic, N. L.; Budinski-Simendic, J.; Ostojic, S.; Kicanovic, M.; Kicanovic, M. B.; Plavsic, M. B. *Mater. Sci. Forum* **2007**, *555*, 473.
29. Raftopoulos, K. N.; Janowski, B.; Apekis, L.; Pielichowski, K.; Pissis, P. *Eur. Polym. J.* **2011**, *47*, 2120.
30. Pavlicevic, J.; Spirkova, M.; Strachota, A.; Mészáros Szécsényi, K.; Lazic, N.; Budinski-Simendic, J. *Thermochim. Acta* **2010**, *509*, 73.
31. Wang, L. F. *Eur. Polym. J.* **2005**, *41*, 293.
32. Rogulska, M.; Kultys, A.; Podkoscielny, W. *Eur. Polym. J.* **2007**, *43*, 1402.
33. Jin-Chao, Z.; Fei-Peng, D.; Xing-Ping, Z.; Wei, C.; Xiao-Mei, W.; Hong, Z.; Xiao-Lin, X.; Yiu-Wing, M. *Compos. B* **2011**, *42*, 2111.
34. Maxwell, J. C. Electricity and Magnetism; Clarendon: Oxford, **1893**.
35. Wagner, K. W. *Arch. Elektrotech.* **1914**, *2*, 371.
36. Sillars, R. W. *Inst. Electr. Eng.* **1937**, *80*, 378.
37. Sauti, G.; McLachlan, D. S. *J. Mater. Sci.* **2007**, *42*, 6477.
38. Hodge, I. M.; Ngai, K. L.; Moynihan, C. T. *J. Non-Cryst. Solids* **2005**, *351*, 104.
39. Pathmanathan, K.; Johari, G. P. *J. Chem. Phys.* **1991**, *95*, 5990.
40. Havriliak, S.; Negami, S. *Polymer* **1967**, *8*, 161.
41. Havriliak, S.; Negami, S. *J. Polym. Sci. Part C: Polym. Symp.* **1966**, *14*, 99.
42. Havriliak, S.; Havriliak, S. J. Dielectric and Mechanical Relaxation in Materials; Hanser: Munich, **1997**, p 57.
43. Donth, E. *J. Polym. Sci. Part B: Polym. Phys.* **1996**, *34*, 2881.
44. Cole, K. S.; Cole, R. H. *J. Chem. Phys.* **1941**, *9*, 341.
45. Boersma, A.; van Turnhout, J.; Wübbenhorst, M. *Macromolecules* **1998**, *31*, 7453.
46. Fragiadakis, D.; Runt, J. *Macromolecules* **2013**, *46*, 4184.
47. Cerveny, S.; Alegría, A.; Colmenero, J. *J. Phys Rev.* **2008**, *E77*, 031803.
48. Capaccioli, S.; Ngai, K. L.; Shinyashiki, N. *J. Phys. Chem.* **2007**, *111*, 8197.
49. Fragiadakis, D.; Runt, J. *Macromolecules* **2010**, *43*, 1028.
50. Vogel, H. Z. *Phys.* **1921**, *22*, 645.
51. Fulcher, G. S. *J. Am. Ceram. Soc.* **1925**, *8*, 339.
52. Tamman, G.; Hesse, W. Z. *Anorg. Allg. Chem.* **1926**, *156*, 245.
53. Lunkenheimer, P.; Kastner, S.; Köhle, M.; Loidl, A. *Phys. Rev.* **2010**, *81*, 051504.
54. Martinez-Garcia, J. C.; Rzoska, S. J.; Drozd-Rzoska, A.; Martinez-Garcia, J. *Nat. Commun.* **2013**, *4*, 1823.
55. Bauer, T.; Lunkenheimer, P.; Loidl, A. *Phys. Rev. Lett.* **2013**, *111*, 225702.
56. Chakrabarty, S.; Karmakar, S.; Dasgupta, C. Annu. Rev. Condens. Matter Phys., **2014**, arXiv:1404.2701 [cond-mat.-stat-mech]. to appear.
57. Lunkenheimer, P.; Schneider, U.; Brand, R.; Loidl, A. *Contemp. Phys.* **2000**, *41*, 15.
58. Böhmer, R.; Ngai, K. L.; Angell, C. A.; Plazek, J. D. *J. Chem. Phys.* **1993**, *99*, 4201.
59. Angell, C. A. *Science* **1995**, *267*, 1924.
60. Angell, C. A. *Polymer* **1997**, *38*, 6261.
61. Angell, C. A. Complex Behavior of Glassy Systems, Proceedings of the XIV Sitges Conference; Sitges: Barcelona, Spain, **1996**.
62. Rubi, M.; Pérez-Vicente, C. Lecture Notes in Physics, Vol. 492. Complex Behavior of Glassy Systems. Proceedings; Barcelona, Spain; Springer: Berlin, **1997**.
63. Doolittle, A. K. *J. Appl. Phys.* **1951**, *22*, 1471.
64. Doolittle, A. K. *J. Appl. Phys.* **1952**, *23*, 236.
65. Bueche, F. *J. Chem. Phys.* **1959**, *30*, 748.
66. Cohen, M. H.; Turnbull, D. *J. Chem. Phys.* **1959**, *31*, 1164.
67. Ferry, J. D. Viscoelastic Properties of Polymers, 2nd ed.; Wiley: New York, **1961**.